applied sciences

MDPI

Article

A Study on the Fracture of Cementitious Materials in Terms of the Rate of Acoustic Emissions in the Natural Time Domain

Dimos Triantis [1,*], Ilias Stavrakas [1], Andronikos Loukidis [1], Ermioni D. Pasiou [2] and Stavros K. Kourkoulis [2]

[1] Electronic Devices and Materials Laboratory, Department of Electrical & Electronics Engineering, School of Engineering, University of West Attica, 250 Thivon Avenue, 122 44 Athens, Greece; ilias@uniwa.gr (I.S.); a.loukidis@uniwa.gr (A.L.)

[2] Laboratory for Testing and Materials, Department of Mechanics, School of Applied Mathematical & Physical Sciences, National Technical University of Athens, Zografou Campus, 157 73 Athens, Greece; epasiou@teemail.gr (E.D.P.); stakkour@central.ntua.gr (S.K.K.)

* Correspondence: triantis@uniwa.gr; Tel.: +30-2105381316

Abstract: A novel approach for describing the acoustic activity in brittle structural materials while they are loaded mechanically at levels close to those causing macroscopic fracture is proposed. It is based on the analysis of the rate of acoustic emissions in terms of the Natural Time concept. Experimental data from protocols with either intact or notched beams, made of cementitious materials, subjected to three-point bending are analyzed. It is concluded that in case the acoustic activity is described with the aid of the F-function in the Natural Time domain, its evolution is governed by a power law, independently of geometrical details and the type of the loading scheme. It appears that the onset of validity of this law provides an interesting pre-failure indicator.

Keywords: cementitious materials; three-point bending; acoustic emissions; natural time; F-function

check for updates

Citation: Triantis, D.; Stavrakas, I.; Loukidis, A.; Pasiou, E.D.; Kourkoulis, S.K. A Study on the Fracture of Cementitious Materials in Terms of the Rate of Acoustic Emissions in the Natural Time Domain. *Appl. Sci.* **2023**, *13*, 6261. https://doi.org/10.3390/app13106261

Academic Editor: Hwa Kian Chai

Received: 8 April 2023
Revised: 14 May 2023
Accepted: 15 May 2023
Published: 20 May 2023

Copyright: © 2023 by the authors. Licensee MDPI, Basel, Switzerland. This article is an open access article distributed under the terms and conditions of the Creative Commons Attribution (CC BY) license (https://creativecommons.org/licenses/by/4.0/).

1. Introduction

A broad variety of experimental techniques has been developed during the last years in order to collect experimental data that could be valuable in the direction of getting deeper insight into the damage mechanisms, which are activated while cementitious building materials are loaded at levels that approach the critical ones, namely, the loads that cause fracture. Among these techniques, the one based on the study of the acoustic emissions (AE) is the technique most broadly used worldwide [1,2].

The AE technique is nowadays the most firmly founded structural health monitoring tool concerning its natural principles. It permits real time monitoring of damage evolution within the mass of loaded materials and structures by detecting the acoustic signals that are emitted as a result of the activation of various mechanisms (like micro-cracking), which release mechanical energy in the form of elastic waves.

Among the simplest parameters, used to study the acoustic activity, is the number of the acoustic signals (either cumulative or not), which are detected and recorded (hits per second). This is a time-dependent function, since micro-cracking becomes gradually more intense as the externally applied load increases approaching the load that will cause macroscopic fracture of the specimen or the structure [3–6].

In this study, the temporal evolution of the acoustic activity is analyzed with the aid of a recently introduced alternative approach, which is based on the F-function [7,8]. Compared to the traditional method of studying the acoustic activity (namely, using directly the "number-of-hits-per-second"), the F-function is proven advantageous since it enlightens with finer resolution the temporal evolution of the acoustic activity, especially during the very last loading steps before macroscopic fracture.

In order for the F-function to be determined and plotted, advantage is taken of the interevent time intervals ($\delta\tau_i$) of a sufficient number n of successive acoustic hits or events. Any specific value of the F-function is the inverse of the average value of the n interevent time intervals. The next value of the F-function is calculated by "sliding" the "window" of the n acoustic signals by one acoustic signal. It can be said, thus, that the F-function represents the average frequency of generation of acoustic hits (or events) from the onset of the loading procedure until the fracture instant. The values of the F-function are "paired" to an average time instant, which is calculated as the mean value (τ) of the time instants at which each one of the n members of the specific "window" were generated (detected). Concerning the numerical value of the parameter n, its choice is, more or less, empirical and depends, mainly, on the overall number N of hits (or events) recorded during the overall duration of the experiment. Usually, n varies between 2% and 10% of N. The study of the acoustic activity by means of the F-function has been already adopted by many researchers worldwide (see indicatively refs. [9–12]).

Very recently the evolution of the F-function was considered in the domain of the Natural Time, χ [13] (instead of the conventional time domain, t), taking advantage of experimental data obtained from a protocol with marble specimens of various geometries subjected to various loading schemes. The concept of Natural Time (NT) was introduced in 2001 by Varotsos et al. [14,15], who suggested that analyzing time series in the NT domain permits the study of the dynamic evolution of complex systems offering valuable insight concerning the proximity to the critical stage, i.e., the stage of impending catastrophic events [16,17]. In this context, it should be noted that acoustic signals emitted in brittle materials, like rocks [18–22], cement mortar [23–25] and polymers [26], have also been analyzed in the Natural Time domain, in an attempt to detect (and if it is possible to predict) the entrance of these materials into their critical stage, i.e., that of impending macroscopic fracture.

Among the most important conclusions of the attempt to analyze the F-function in terms of the Natural Time χ [13], was that, during the last loading stages before macroscopic fracture, the acoustic activity is governed by a power law of the form:

$$F(\chi) = A \cdot \chi^m \quad (1)$$

where m is an exponent characterizing the intensification of the acoustic activity just before the final fracture and A is a numerical constant. Both A and m are determined by a proper curve fitting procedure.

The present study is part of a wider project, the aim of which is to investigate the existence and applicability of pre-failure indices, i.e., indices that could be considered as signals, timely warnings about upcoming catastrophic failures. In this direction, the specific motive of the study is to check whether the characteristic power law, which was proven to govern the mechanical response of marble specimens [13] at the stages of impending fracture, is applicable to other classes of materials. The critical novelty of the study is that the response of the materials is considered in the Natural Time domain rather than in the conventional time domain. In this context, the procedure introduced in ref. [13] is here extended to cover a broader variety of brittle materials. More specifically, beam-shaped specimens, either intact or notched, made of cement mortar (either plain or reinforced), are subjected to three-point bending. The acoustic activity recorded is analyzed in the NT domain, in terms of the F-function, the determination of which is here slightly modified, compared to that adopted in ref. [13].

2. The Rate of Generation of Acoustic Hits (F-Function) in the Natural Time Domain

Assume that, during the loading procedure, i.e., from the onset of loading until the fracture of the specimen, N acoustic hits are recorded at the time instants $t_1, t_2, \ldots, t_i, \ldots, t_N$. The respective time series, expressed in terms of the Natural Time, χ, is denoted as: $\chi_1 = \frac{1}{N}, \chi_2 = \frac{2}{N}, \ldots, \chi_i = \frac{i}{N}, \ldots, \chi_N = \frac{N}{N} = 1$. Along the same lines, the respective N values of the load applied at each time instant t_i are recorded and denoted as

$\ell_1, \ell_2, \ldots, \ell_i, \ldots, \ell_N$. In order to calculate the values of the F-function, the interevent time intervals $\delta\tau_i = t_i - t_{i-1}$, are used, where t_i and t_{i-1} are the instants at which any two successive AE hits were recorded.

Denoting, as already mentioned, by $\delta\tau_i = t_i - t_{i-1}$ the interevent time, i.e., the time interval between two successive acoustic hits, then the quantity $f_i = \frac{1}{\delta\tau_i} = \frac{1}{t_i - t_{i-1}}$ represents the instantaneous frequency of generation of acoustic hits when the i_{th} hit is recorded. Taking advantage of the instantaneous frequencies f_i of n successive acoustic hits, the respective value of the F-function is determined as follows:

$$F_i = \frac{\sum_{j=i-n+1}^{j=i} f_j}{n} \tag{2}$$

Sliding by one acoustic hit the "window" of the n successive acoustic hits the next value of the F-function is obtained and so on. Any specific value of the F-function is paired to the average value (τ) of the time instants at which the n successive acoustic hits of the specific "window" were recorded. It is thus evident that the F-function is in fact a time series of m = N − n + 1 discrete values of F(τ) and can be plotted graphically along the time parameter τ.

As a next step, each value of the time parameter τ_i is paired to a Natural Time "instant" X_i and a load value L_i, according to the following scheme:

$$\tau_i = \frac{\sum_{j=i-n+1}^{j=i} t_j}{n} \rightarrow X_i = \frac{\sum_{j=i-n+1}^{j=i} \chi_j}{n} \rightarrow L_i = \frac{\sum_{j=i-n+1}^{j=i} \ell_j}{n} \tag{3}$$

Therefore, instead of the time series F(τ), with m = N − n + 1 discrete values, the corresponding time series F(X) and L(X) are obtained in the Natural Time domain and can be plotted in juxtaposition to each other in the same graph. In case the load is not recorded simultaneously with the acoustic hit, but rather it is recorded from an "independent" sampling technique, using a different hardware, then it is possible to apply the above-described procedure with the aid of the table of values $X_i(\tau_i)$ by means of interpolation. The above procedure is schematically described in Table 1.

Table 1. The procedure to convert the F(τ) time series to the respective F(X) and L(X) time series. Green color indicates the Group of n successive values of the acoustic hits.

	N Values of Acoustic Hits									
Time (t)	t_1	t_2	....	t_n	....	t_{i-n+1}	....	t_i	....	t_N
						n successive values of acoustic hits				
Load (ℓ)	ℓ_1	ℓ_2	....	ℓ_n		ℓ_{i-n+1}	....	ℓ_i	....	ℓ_N
IT ($\delta\tau$)	$\delta\tau_1 = t_1$	$\delta\tau_2$	....	$\delta\tau_n$	....	$\delta\tau_{i-n+1}$	....	$\delta\tau_i = t_1 - t_{i-1}$	....	$\delta\tau_N$
f	f_1	f_2	....	f_n	....	f_{i-n+1}	....	$f_i = \frac{1}{\delta\tau_i}$	....	f_N
NT (χ)	$\chi_1 = \frac{1}{N}$	$\chi_2 = \frac{2}{N}$	....	$\chi_n = \frac{n}{N}$	....	χ_{i-n+1}	....	$\chi_i = \frac{i}{N}$	....	$\chi_N = 1$
	Calculating the (N – n + 1) values of the F-function and of the Load (L) vs the Natural Time (X)									
	F function			$F_n = \frac{\sum_{j=1}^{j=n} f_j}{n}$	....	F_{i-n+1}	....	$F_i = \frac{\sum_{j=i-n+1}^{j=i} f_j}{n}$	....	$F_N = \frac{\sum_{j=N-n+1}^{j=N} f_j}{n}$
	Time (τ)			$\tau_n = \frac{\sum_{j=1}^{j=n} t_j}{n}$	....	τ_{i-n+1}	....	$F_i = \frac{\sum_{j=i-n+1}^{j=i} f_j}{n}$	....	$\tau_N = \frac{\sum_{j=N-n+1}^{j=N} t_j}{n}$
	NT (X)			$X_n = \frac{\sum_{j=1}^{j=n} \chi_j}{n}$	....	X_{i-n+1}	....	$X_i = \frac{\sum_{j=i-n+1}^{j=i} \chi_j}{n}$	....	$X_N = \frac{\sum_{j=N-n+1}^{j=N} \chi_j}{n}$
	Load (L)			$L_n = \frac{\sum_{j=1}^{j=n} \ell_j}{n}$	....	L_{i-n+1}	....	$L_i = \frac{\sum_{j=i-n+1}^{j=i} \ell_j}{n}$	....	$L_N = \frac{\sum_{j=N-n+1}^{j=N} \ell_j}{n}$

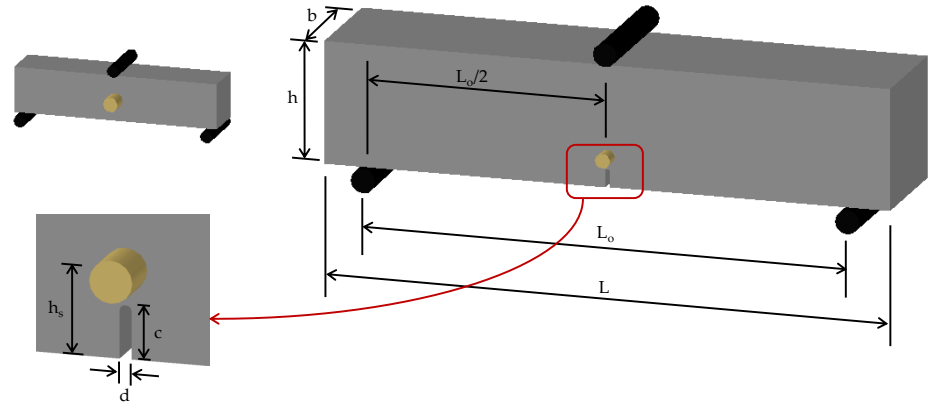
It is concluded that the procedure for converting the time series from the conventional time domain to the respective ones in the Natural Time domain adopted here, is not identical to that adopted in ref. [13], in which the first value of the Natural Time, χ_1, was paired to the first value of the F-function and the last value, χ_N, to the last value of the F-function. In this study, the Natural Time starts counting simultaneously with the generation of the first acoustic hit. Similarly, when the last (N_{th}) acoustic hit is generated (i.e., at the instant of the macroscopic fracture) the respective value X_N of the Natural Time is determined as:

$$X_N = \frac{\sum_{j=N-n+1}^{j=N} \chi_j}{n} \quad (4)$$

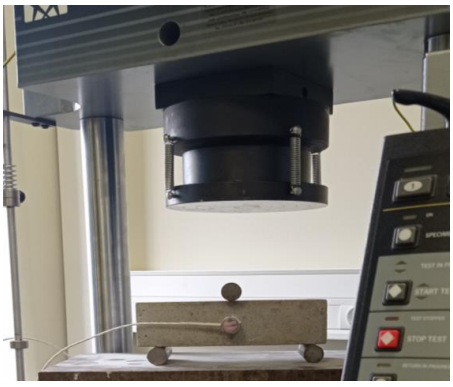
which is not exactly equal to 1, but rather it attains a value which tends to 1. The two approaches for converting the time series from the conventional time domain to that of the Natural Time will be considered comparatively in the next sections. It will be proven that the differences are of rather marginal importance.

3. The Specimens and the Experimental Protocols

In this study, advantage is taken of the data provided by two experimental protocols. The first one included intact beam-shaped specimens of relatively small dimensions (i.e., length equal to 250 mm and square cross section equal to 55 × 55 mm^2). The specimens were subjected to three-point bending adopting load-control conditions at two rates equal to 66 N/s and 80 N/s (Figure 1a). The distance between the supporting rollers was equal to 220 mm (Figure 1a). A photo of a typical specimen while loaded is shown in Figure 1b.



(**a**)



(**b**)



(**c**)

Figure 1. (**a**) The geometry of the specimens used. Upper row left: Intact specimens. Upper row right: Notched specimens. The distance of the center of the acoustic sensor from the bottom face of the specimen was equal to h = 35 mm. (**b**) Photo of an intact specimen just before loading. (**c**) Photo of a notched specimen during the loading procedure.

The specimens were prepared using Ordinary Portland cement and fine aggregates with average dimensions ranging from 0.6 mm to 3 mm. The "cement/aggregate/water" ratio was equal to 2/6/1 (by weight). The compressive strength was equal to about 32 MPa, while the respective tensile one (as determined by splitting tests, i.e., Brazilian-disc tests) was equal to about 3.0 MPa.

In the next section the data gathered during two typical tests of this protocol will be analyzed: The first one is the test encoded as LR1: The loading rate was equal to 66 N/s, and fracture occurred at a load level equal to $L_{max,LR1} \approx 3.74$ kN. The second one is the test encoded as LR2: The loading rate was equal to 80 N/s, and fracture occurred at a load level equal to $L_{max,LR2} \approx 3.87$ kN.

The second protocol included beam-shaped specimens of significantly larger dimensions (length equal to L = 700 mm and square cross-section equal to hxb = 150 × 150 mm^2). The specimens were notched at their central section (normally to their longitudinal axis) by means of a rotating disc. The depth of the notches was equal to c = 25 mm while their width (breadth) was equal to about d = 5 mm. The specimens were subjected to three-point bending (Figure 1a) adopting displacement-control conditions at a rate equal to 0.08 mm/min with the aid of a stiff servo-hydraulic INSTRON-SATEC frame of capacity equal to 300 kN. The distance between the supporting rollers was equal to L_o = 600 mm. A photo of a typical specimen while loaded is shown in Figure 1c.

Again, two typical tests of this protocol will be analyzed in the next section. In the first one, the specimen (encoded as R0) was unreinforced (similar composition to the specimens of the previous protocol), and the maximum load attained was equal to L_{max} = 11.70 kN, while in the second one the specimen (encoded as RM) was reinforced with short metallic fibers at a portion of 25 kg/m^3. Round steel fibers were used, the diameter and length of which were equal to about 1.30 mm and 50 mm, respectively. Their tensile strength is around 690 MPa. The maximum load attained for this specimen was equal to L_{max} = 14.05 kN.

For both protocols the acoustic signals were detected using an acoustic sensor, properly mounted at the plane along which crack propagation was expected, using a layer of silicon grease to optimize contact. The acoustic sensor used in the experimental protocol was the R15α, the resonant frequency and the operating frequency of which are 75 kHz and 50–400 kHz, respectively. The PCI-2 AE system with a preamplifier of 40 dB (Mistras Group, Inc., West Windsor Township, NJ, USA) was used to record and store the experimental data. A threshold of 40 dB was set, together with a low-frequency cutting filter, in order to exclude signals of frequency lower than 20 kHz.

4. Experimental Results and Discussion

4.1. Intact Cement Mortar Specimens under Three-Point Bending

For the specimen loaded at a constant rate equal to 66 N/s (specimen LR1), a number of N = 580 acoustic hits were recorded until the fracture instant. The temporal evolution of the load applied is plotted in Figure 2a, in juxtaposition to that of the amplitude of the acoustic hits. The fracture instant was detected at t_f = 56.3 s. The respective evolution of these quantities in the Natural Time domain is plotted in Figure 2b. In this figure, each acoustic hit is located at a "distance" equal to $\Delta\chi = 0.0017$ from the two neighbor acoustic hits (i.e., the one at the left and the one at the right).

Adopting now the methodology described in Section 2 (Table 1), the values of the F-function were calculated using a sliding window of n = 15 successive interevent times, and each value was associated to a unique value of the Natural Time X. In this way, it became possible to plot the evolution of the F-function and also, of the Load, versus the Natural Time parameter, X, as it is seen in Figure 3. In this figure the short, thick, blue, linear segment represents the very last value of the F-function, which corresponds to the width of the sliding window of the last n = 15 acoustic hits recorded before macroscopic fracture (i.e., from χ_{N-n+1} to χ_N).

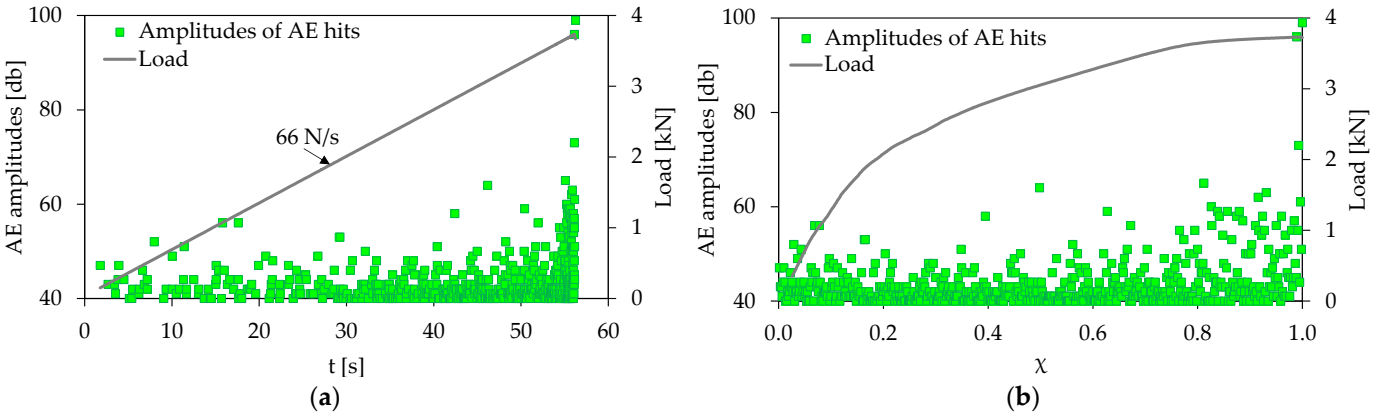


Figure 2. The temporal evolution of the load applied, in juxtaposition to that of the amplitude of the acoustic hits, in (**a**) the conventional- and (**b**) the Natural-Time domains, for the LR1 test.

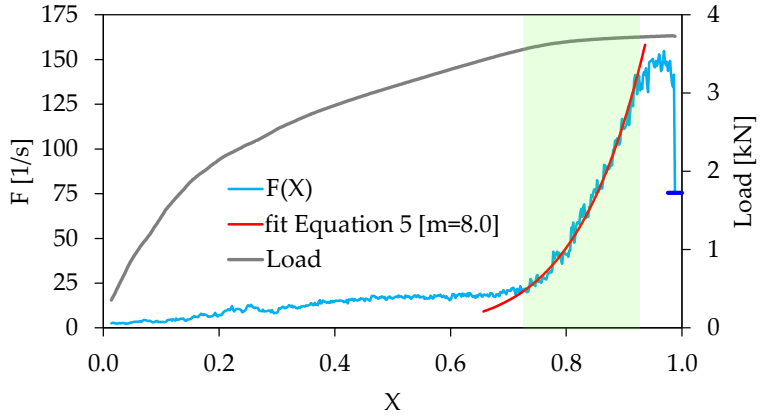


Figure 3. The evolution of the F-function versus the Natural Time X in juxtaposition to the respective evolution of the Load applied for the LR1 test.

It is obvious from Figure 3, that, in the $0.72 < X < 0.92$ interval (see the green-shaded rectangle), the F-function is almost perfectly governed by a power law of the form:

$$F(X) = A \cdot X^m \quad (5)$$

The fitting procedure (red line in Figure 3) provides for the exponent m a numerical value equal to m = 8.0. It is worth noticing that, in this region of X-values, the load applied increases from about 95% to almost 99% of the maximum value attained before macroscopic fracture ($L_{max} \approx 3.74$ kN). As mentioned previously, fracture occurred at the instant $t_f = 56.3$ s and, therefore, the time interval $0.72 < X < 0.92$ corresponds to the time interval $0.4 \text{ s} < t_f - t < 2.9$ s. As a first conclusion, it can be said that the rapid increase of the F-function, observed a few seconds before fracture, is described excellently by the power law given by Equation (5), which is identical to the law suggested in ref. [13] for a completely different material. This conclusion is in full accordance with the findings of Wang et al. [10], who studied the response of concrete specimens and concluded that, at the stage of the accelerated growth of microcracks, the F-function starts increasing, rapidly attaining its maximum value. Moreover, it is quite interesting to note that, at the specific interval of X-values (i.e., the $0.72 < X < 0.92$ interval), additional quantities (as for example the cumulative counts) appear being governed by a similar power law in case their evolution is described in the Natural Time domain. Further details concerning the evolution of the cumulative counts will be given in Section 5 (Discussion and Concluding remarks).

The procedure adopted for the analysis of the data of the LR1 test is now applied for the study of the LR2 test, in which the specimen was loaded at a higher rate, equal to 80 N/s. In

this test, N = 734 acoustic hits were recorded until the time instant of macroscopic fracture. The temporal evolution of the load applied is plotted in Figure 4a, again, in juxtaposition to the amplitude of the acoustic hits. The fracture instant was detected at t_f = 45 s. The respective evolution of both quantities (load and amplitude of the acoustic hits) in the Natural Time domain is plotted in Figure 4b. In Figure 4b each acoustic hit is "located' at a "distance" equal to $\Delta\chi$ = 0.0014 from its neighbor hits (i.e., that at the left and that at the right).

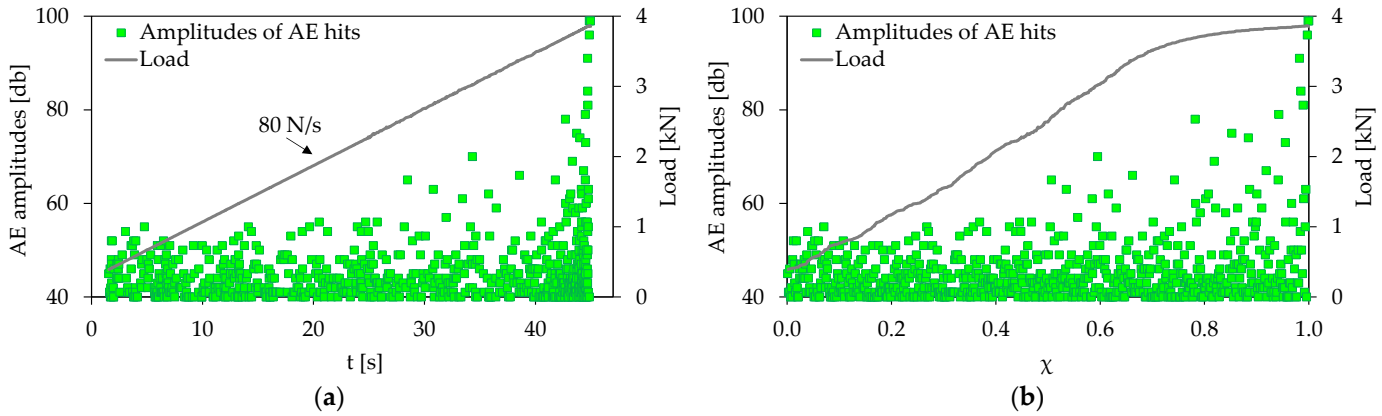


Figure 4. The temporal evolution of the load applied, in juxtaposition to that of the amplitude of the acoustic hits in (**a**) the conventional- and (**b**) the Natural-Time domains, for the LR2 test.

For the specific test, the determination of the values of the F-function was implemented using n = 20 successive interevent time intervals. Then these values were associated to the respective values of the Natural Time, X. The evolution of the F-function and, also, of the Load, versus the Natural Time parameter is now plotted in Figure 5. In Figure 5 the short, thick, blue, linear segment represents, again, the last value of the F-function, corresponding to the width of the sliding window of the last n = 20 acoustic hits recorded before macroscopic fracture (i.e., from χ_{N-n+1} to χ_N).

Again, it is definitely concluded that the power law of Equation (5) governs faithfully the evolution of the F-function in the 0.65 < X < 0.94 region (see the bright green rectangle in Figure 5). In this region the load increases from about 87% to about 99% of the respective maximum value attained before macroscopic fracture ($L_{max} \approx$ 3.87 kN). As mentioned previously, fracture occurred at the instant t_f = 45.0 s, and, therefore, the time interval 0.72 < X < 0.92 corresponds to the time interval 0.3 s < $t_f - t$ < 6.3 s. The curve-fitting procedure (red line in Figure 5) provides for the parameter m a numerical value equal to m = 6.6.

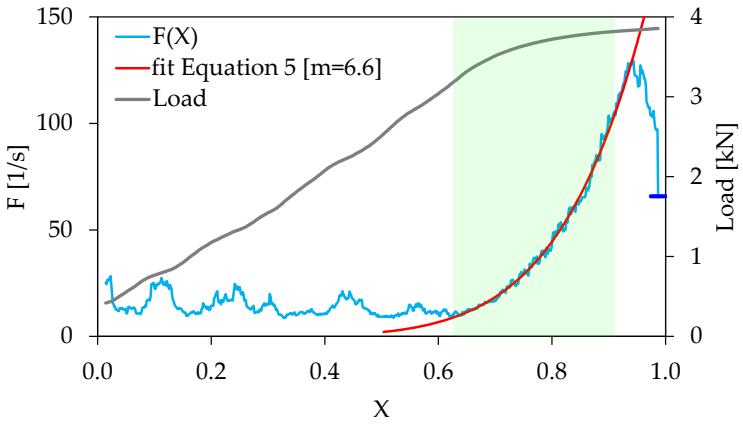


Figure 5. The evolution of the F-function versus the Natural Time X in juxtaposition to the respective evolution of the Load applied, for the LR2 test.

4.2. Notched Cement Mortar Beams under Three-Point Bending

4.2.1. Unreinforced Specimen (R0)

During this test N = 929 acoustic hits were recorded until the instant of macroscopic fracture. The temporal evolution of the load applied is plotted in Figure 6a, in juxtaposition to the evolution of the amplitude of the acoustic hits recorded. (It is recalled that the specimen is now loaded under displacement-, rather than load-, controlled conditions; therefore, the load-time curve is not linear.) The overall duration of the specific test was equal to t_f = 990 s, and the macroscopic fracture was rapid and almost instantaneous. Indeed, it was only 2 s before the rapid load drop that the load exhibited a slight decreasing trend.

The respective evolution of the load and that of the amplitude of the acoustic hits in the Natural Time domain is plotted in Figure 6b. Each hit is located at a "distance" equal to $\Delta\chi \approx 0.0011$ from its two neighbor acoustic hits. Considering that the maximum load attained was equal to L_{max} = 11.7 kN and it corresponds to a natural time χ = 0.53, it is concluded that the acoustic hits recorded until the load attained its peak value are only equal to 50% of the overall number of acoustic hits recorded. The remaining 50% of the acoustic hits are recorded during the very short interval of gradual load decrease, the duration of which is equal to only 2 s before macroscopic fracture.

The evolution of the F-function, in terms of the Natural Time X, is plotted in Figure 7, again in juxtaposition to that of the load applied L(X). For the specific test, the values of the F-function were calculated using a sliding window of n = 50 successive interevent times. The thick, blue, linear segment, corresponding to the last value of the F-function, denotes, as previously, the last "window", i.e., the last n = 50 values of the Natural Time (χ).

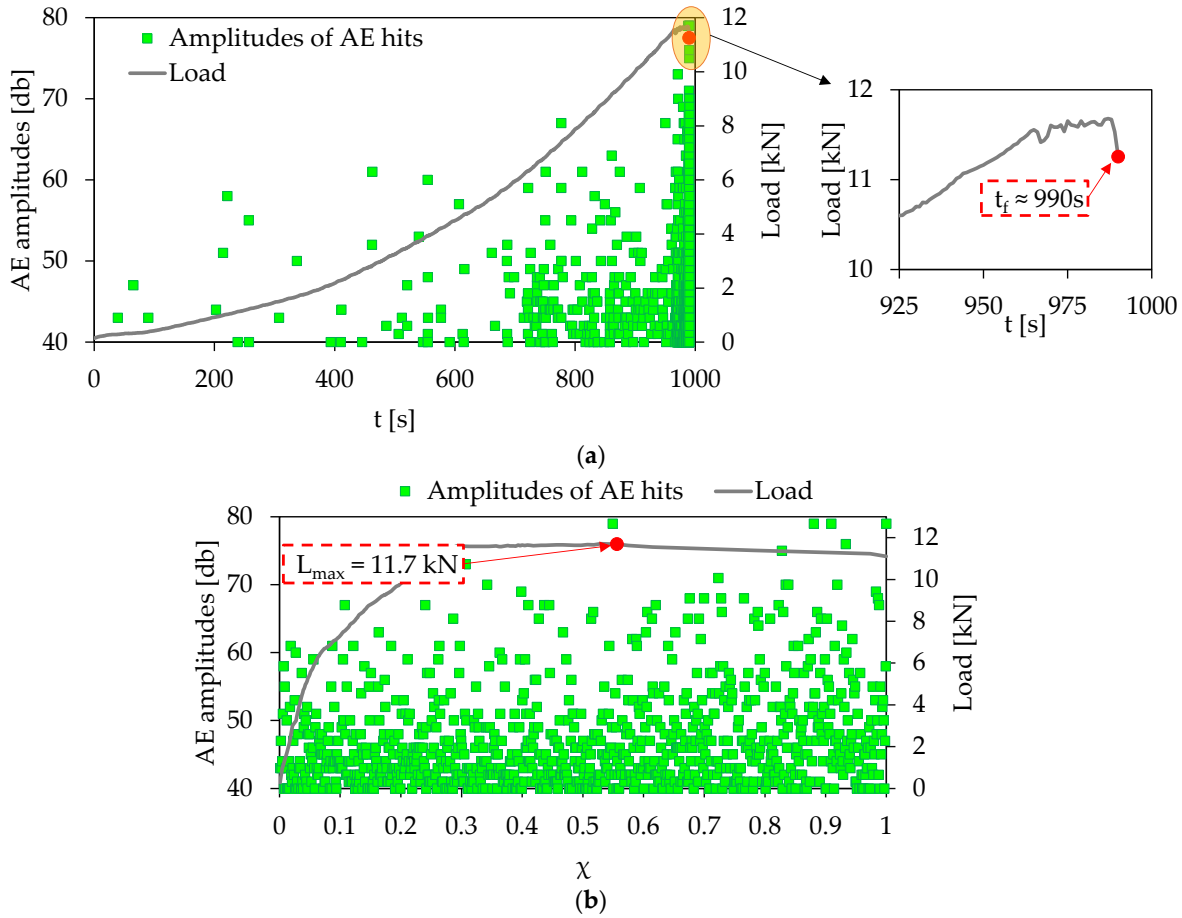


Figure 6. The temporal evolution of the load applied, in juxtaposition to that of the amplitude of the acoustic hits in (**a**) the conventional- and (**b**) the Natural-Time domains for the R0 test.

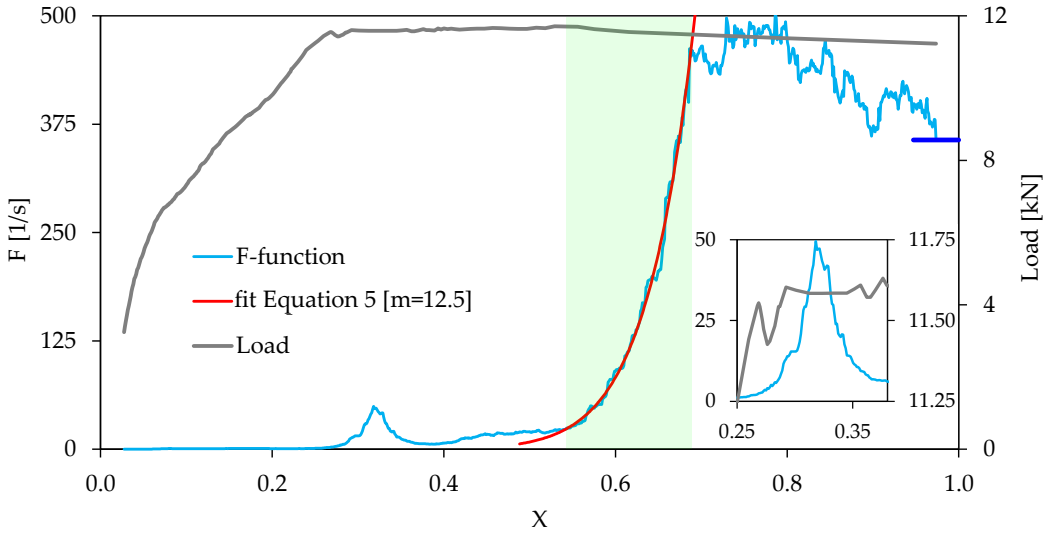


Figure 7. The evolution of the F-function versus the Natural Time X in juxtaposition to the respective evolution of the Load applied for the R0 test.

In Figure 7 it is observed that the F(X)-function starts increasing rapidly at X = 0.55 and keeps increasing until X = 0.69 (see the bright green rectangle in Figure 7). The power law of Equation (5) governs again, excellently, the evolution of the F-function in this interval of rapid increase, and the respective numerical values of the exponent m is equal to m = 12.5. It is worth observing that, in the above interval of X-values, the load applied has attained its peak value and has, already, started decreasing, although according to an almost imperceptible manner. Therefore, this rapid increase of the F-function, in the specific time interval, designates the upcoming fracture of the specimen or, in other words, its entrance into the critical stage (that of impending fracture).

Finally, it is worth indicating the existence of a local maximum of the F(X) at the $0.29 < X < 0.36$ interval, which is related to a premature load decrease (as it is seen in the figure embedded in Figure 7). This observation may be related to a local non-critical fracture (perhaps a local exfoliation observed in the vicinity of the one of the two supporting metallic rollers). Although the percentage of acoustic hits in this X-interval is not significant, it is observed that acoustic signals with low interevent time intervals are detected, which results in increased values of the F-function.

4.2.2. Specimen Reinforced with Short Metallic Fibers (RM)

The main difference of the specific test, compared to all tests described until now, is that there is not a uniquely defined fracture instant or, equivalently, there is not an instant at which the load is zeroed. Indeed, the presence of the reinforcing fibers prohibits the rapid propagation of the macroscopically visible crack front. This is clearly seen in Figure 8a, in which the temporal evolution of the load applied is plotted, in juxtaposition to the respective evolution of the amplitude of the acoustic hits recorded (again it is recalled that the specimen is loaded under displacement-control conditions): At the instant t = 1519 s, the load attains its maximum value, equal to $L_{max} \approx 14.05$ kN. Then the load remains practically constant until the instant t = 1524 s, and it starts decreasing relatively smoothly (while the crack front has not yet started propagating) until the instant t_f = 1531 s, indicating the "ductility" gained by the specimen, due to the presence of the metallic reinforcing fibers.

This gain in ductility of the otherwise "brittle" concrete is a common feature and, besides the increase in strength, is the main reason for adding the reinforcing fibers [27–32]. After this instant t_f, the load decreases abruptly to a level equal to about 9 kN, at which it remains almost constant for a relatively long time-interval, during which the macrocrack is propagating steadily. The instant t_f is considered here as a "conventional fracture instant" (although the specimen is not fragmented into two pieces) since after the instant

t_f the crack front is moving very slowly from the crown of the notch towards the load transferring roller. The number of acoustic hits recorded until the instant t_f was equal to N = 2598 (more than two times the hits recorded in the test with the unreinforced specimen, R0). Although comparing the number of AE hits recorded in two different tests is perhaps not a good practice, it provides some interesting conclusions (of qualitative nature) in case of identical specimens. In this case, the conclusion is definitely justified taking into account the additional damage mechanism activated, namely the debonding between the concrete matrix and the reinforcing fibers.

The evolution of the above two quantities (load and amplitude of the acoustic hits) in natural time, χ, is plotted in Figure 8b. Each acoustic hit is now located at a "distance" equal to $\Delta\chi \approx 3.85 \times 10^{-4}$ from its right and left neighbors. The instant at which the load is maximized corresponds to a natural time equal to $\chi = 0.60$. Almost 60% of the acoustic hits were recorded until this instant, i.e., until maximization of the load applied.

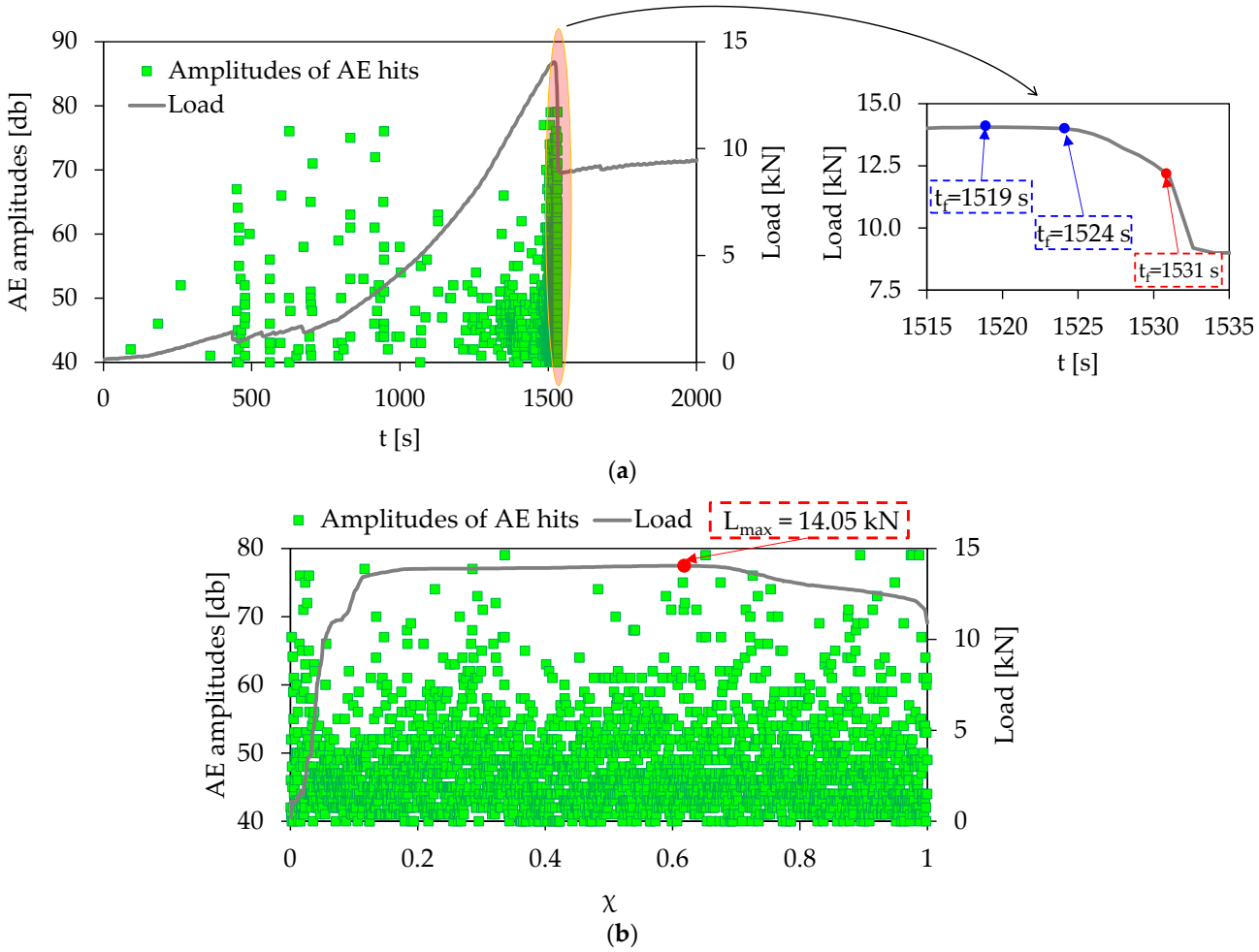


Figure 8. The temporal evolution of the load applied, in juxtaposition to that of the amplitude of the acoustic hits, in (**a**) the conventional- and (**b**) the Natural-Time domains for the RM test.

Concerning now the evolution of the F-function, in terms of the Natural Time X, it is plotted in Figure 9, in juxtaposition to that of the load applied L(X). For this to be achieved, the F-function was calculated using a sliding window of n = 50 successive interevent times. The short, thick, blue linear segment, corresponding to the last value of the F-function, denotes, again, the last "window", i.e., the last n = 50 values of the Natural Time (χ).

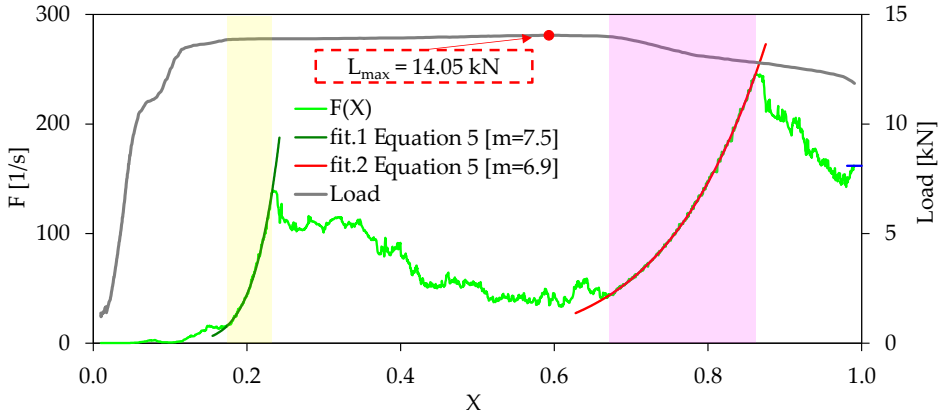


Figure 9. The evolution of the F-function versus the Natural Time X in juxtaposition to the respective evolution of the Load applied, for the RM test.

It is seen from Figure 9 that, for this specimen, there are two X-intervals at which the F-function is governed by the power law of Equation (5). The first one is the $0.17 < X < 0.24$ interval (yellow-colored rectangle in Figure 9). For this first interval, the fitting procedure (dark green line) provides a numerical value for the exponent m equal to m = 7.5. In this interval, the load increases imperceptibly (in fact it is almost constant) from 13.8 kN to about 13.9 kN, i.e., the load is almost equal to about 98.5% of the maximum value attained (L_{max} = 14.05 kN).

The second interval at which the law of Equation (5) becomes dominant is the $0.67 < X < 0.86$ one (magenta-colored rectangle in Figure 9). In this interval, the load has already started decreasing very smoothly from a maximum value of about 14.05 kN towards a value of about 13.9 kN. It is worth mentioning that the X = 0.86 instant corresponds to only 2 s before the abrupt load drop, i.e., the conventional fracture instant. For this second interval the fitting procedure (red line) provides a numerical value for the exponent m equal to m = 6.9.

5. Discussion and Concluding Remarks

5.1. Comparative Consideration of the Tests with Intact Beams (Tests RL1 and RL2)

The results for the two tests with intact specimens (specimens of identical composition, subjected to the same loading scheme but under different loading rates) are considered comparatively in Figure 10, in which the two F(X) functions are plotted in juxtaposition to each other. It can be seen from Figure 10 that, in case the beam is subjected to a higher loading rate (80 N/s), the acoustic activity until the instant with $X < 0.3$ (or equivalently for $L < 1.55$ kN) is clearly stronger compared to that of the beam subjected to a lower loading rate (66 N/s). In addition, the evolution of the F-function for the test with the higher loading rate is not smooth but rather it is characterized by relatively strong fluctuations. It appears, therefore, that increased loading rates are associated with earlier onset of micro-cracking, almost simultaneously with the onset of the loading procedure. On the contrary, for lower loading rates, one observes a smooth and gradually increasing rate of generation of micro-cracks. For both cases, a global maximum is attained by the F(X)-functions, a little before macroscopic fracture. This global maximum is followed by a gradual decrease, which is attributed to the fact that the interevent time intervals ($\delta\tau_i$) between the acoustic hits are now characterized by longer duration (and higher energy content) [8,33].

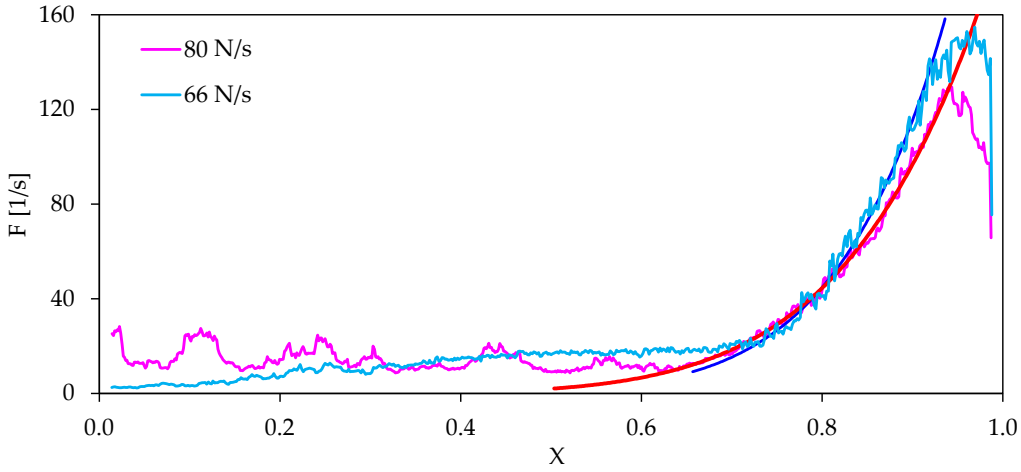


Figure 10. Comparative consideration of the evolution of the F-functions in the Natural-Time Domain for the specimens of the protocol with intact specimens. The dark blue and the dark red lines correspond to the parts of the F-function which obey the power law of Equation (5).

In addition, it is interesting to observe that, at the last loading stages, the values of the F-function corresponding to the specimen subjected to lower loading rate exceed the respective values of the specimen subjected to higher loading rate. This observation could be explained by taking into account that increased loading rates correspond to earlier activation of the damage mechanisms responsible for micro-cracking (or in other words, for rapidly increasing values of the F-function), or equivalently their action is spread over a longer time interval (either in the conventional or in the Natural-Time domain) since, as it was mentioned, their activation is almost simultaneous to the onset of loading.

In order to further enlighten this issue, the evolution of the load applied at the intervals where the power law of Equation (5) is valid is plotted in Figure 11 (thick lines), both in terms of the Natural Time (Figure 11a) and also in terms of the conventional time (Figure 11b).

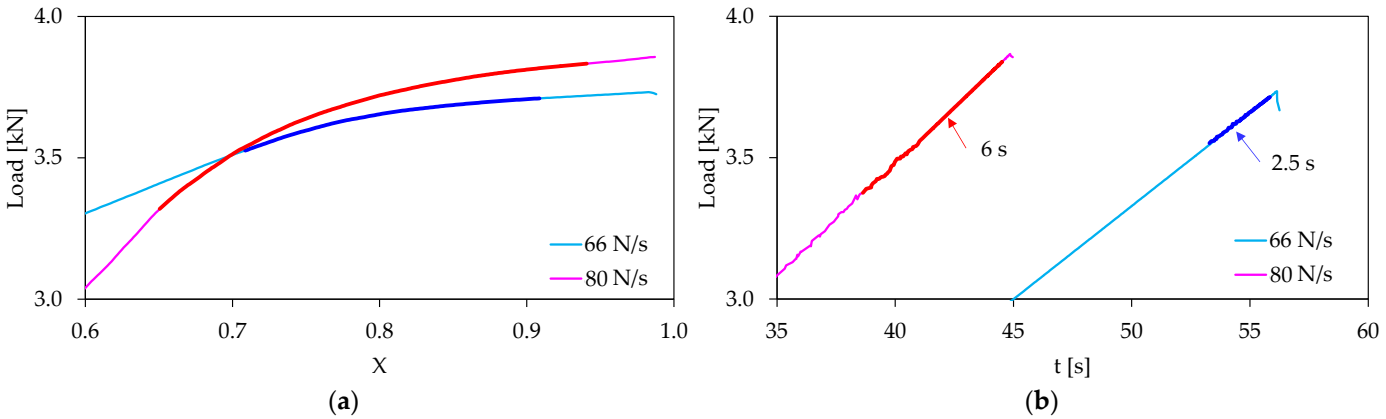


Figure 11. Magnified view of the intervals where the law of Equation (5) is valid (thick lines), in terms of the Natural Time (**a**) and the conventional time (**b**) for the protocol with intact specimens.

Comparing the two figures it is seen that, for the beam loaded at the higher rate, the duration of the interval of intense increasing is significantly longer compared to that of the beam loaded at the lower rate.

5.2. Comparative Consideration of the Tests with Notched Beams (Tests R0 and RM)

For both notched specimens (unreinforced and reinforced with metallic fibers), the overall evolution of the F(X)-function exhibits some common characteristics. The first

one is that severe increase of the values of the F(X)-function (and therefore of the rate of micro-cracking) is observed while the load applied approaches closely its maximum value (but before this value is attained) (Figure 12a). This interval is denoted from here on as Region I.

In addition, the values of the F(X)-function increase rapidly, obeying a power law, also a little before the instant of macroscopic fracture (either actual or "conventional"), while the load applied has already attained its maximum value and has started decreasing very smoothly. This interval is denoted from here on as Region II. In this interval, one observes the most intense generation of acoustic hits, or equivalently the most intense micro-cracking procedure. Both Regions (I and II) of intense micro-cracking are plotted with thick red line in Figure 12, in which the evolution of the load applied (Figure 12a) and that of the F-function (Figure 12b) is plotted in the Natural Time domain, for both the unreinforced and the reinforced beams.

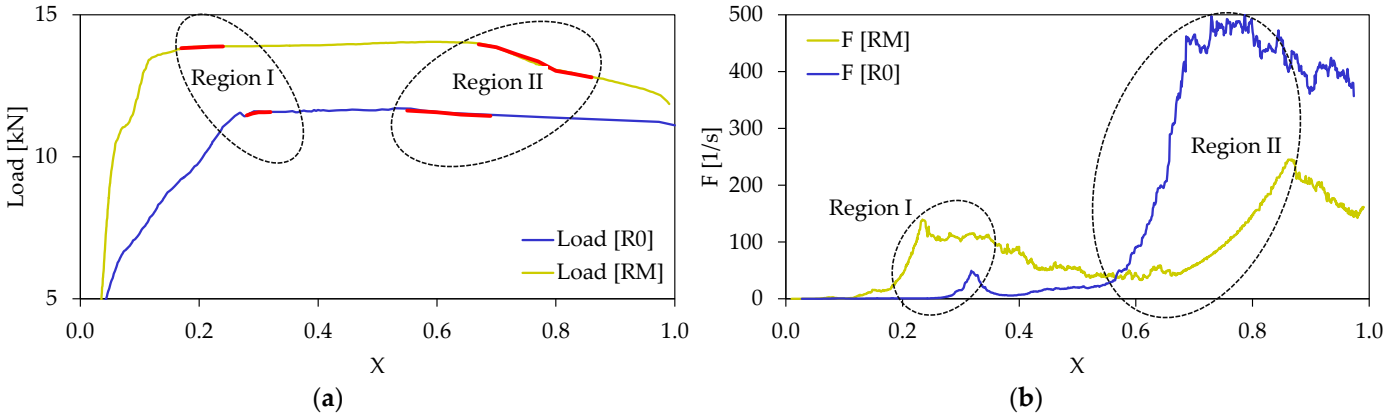


Figure 12. Comparative consideration of the evolution of the load (**a**) and of the F-function (**b**) in the Natural Time domain for the protocol with notched specimens. The thick red lines correspond to the portions of the load plot for which the respective F-function is described by the power law of Equation (5).

Concerning Region I, the F(X) function exhibits significantly higher values in the case of the reinforced specimen (Figure 12b). This is attributed to the increased number of micro-cracks developed due to the fact that there are damage mechanisms activated both in the bulk of the material and also along the mortar-fibers interfaces (which do not exist in the unreinforced specimen).

On the contrary, things are completely different for Region II. The values of the F(X)-functions are now quite significantly higher for the unreinforced beam (test R0). This is obviously due to the fact that the intense acoustic activity in the plain beam has a much shorter duration compared to the respective duration in the reinforced beam. This is explained by the presence of the metallic reinforcing fibers, which offer an increased "ductility" to the beam. This is even more evident if one is "transferred" from the Natural Time Domain X to that of the conventional time τ and considers comparatively (for the reinforced and the unreinforced specimens) the respective evolution of the F(τ)-functions and that of the Load applied (L(τ) functions). The results for the very last loading stages (i.e., just before fracture) are plotted in Figure 13.

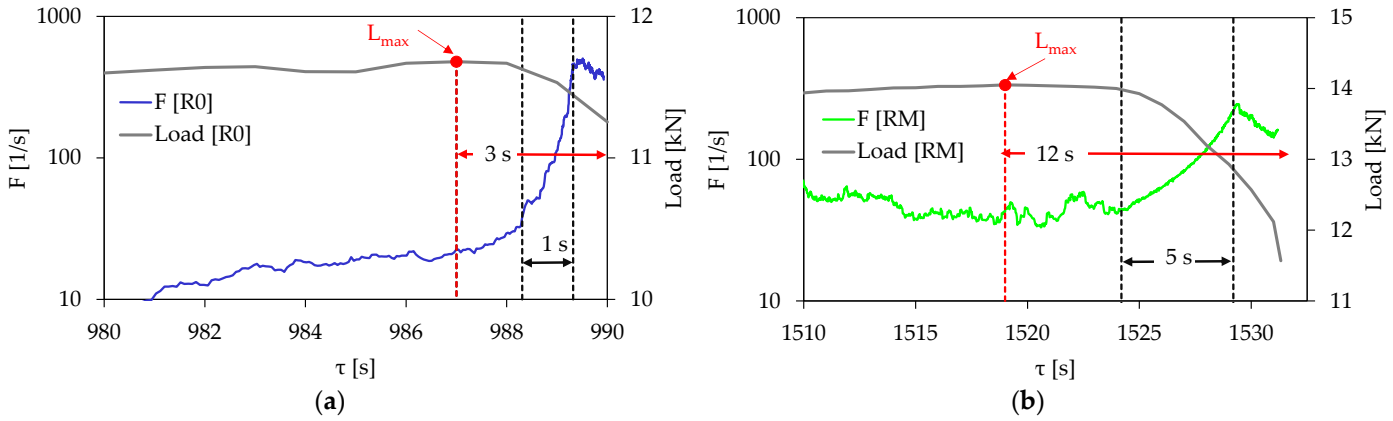


Figure 13. The evolution of the F-function and the load applied, in the conventional time domain, for the unreinforced (**a**) and the reinforced (**b**) notched specimens, during an interval of a few seconds before macroscopic fracture.

It is observed from this figure that, for the R0 beam, the interval at which the F(τ)-function exhibits rapid increase has a duration equal to about only 1 s. On the other hand, for the RM beam, the respective duration is equal to about 5 s. Moreover, from the same Figure 13a,b, it is observed that at the interval during which the load oscillates (remaining practically constant) around the maximum value attained, the values of the F-function for the RM beam are equal to about 50 hits/s, while for the R0 beam, the respective values increase from the level of 10 hits/s to the level of 30 hits/s. In addition, the time interval from the instant at which the load attains its maximum value until the instant of macroscopic fracture is only 3 s for the R0 beam and 12 s for the RM one. As a result, the presence of the metallic fibers in the reinforced beam, RM, prolongs the interval before the generation of the fatal macro-crack, and although an increased number of acoustic hits is recorded, the maximum value of the F-function is quite lower compared to that of the unreinforced beam, R0.

5.3. Comparative Consideration of the F(χ) and F(X) Approaches for the Determination of the Time Series in Natural Time

As already mentioned, a modified procedure was adopted in this study, for the interpretation of the acoustic activity in the Natural Time domain, compared to the respective one used in ref. [13], in which experimental protocols with marble specimens were analyzed. The difference is that, in the present study, the Natural Time, χ, starts counting simultaneously with the generation of the first acoustic hit. Taking into account that the first value of the F-function is calculated after recording the n first hits, the correlation of the F-function to the Natural Time is here achieved in terms of the X- (rather than the χ-) parameter, which is the average of the χ-values of the first n acoustic hits recorded. As an obvious result, the last X-value is not exactly equal to 1 (it rather tends to this value) since it is calculated by the n acoustic hits recorded last. Recapitulating and contrary to what was adopted here, in the previous study (ref. [13]), the Natural Time started counting from the time instant at which the first value of the F-function was calculated, i.e., after the n first hits were recorded.

However, considering comparatively the outcomes of the two approaches, it can be concluded that the differences are of minor importance and of quantitative rather than qualitative nature.

The above conclusions are clearly seen in Figure 14 in which the evolution of the F-function, either in terms of the X- (Figure 14a) or in terms of the χ-parameter (Figure 14b), for the unreinforced beam, R0, is presented. Minor, quantitative only, discrepancies are observed, which concern mainly the numerical values of the fitting parameters, as it can be seen in Table 2. The critical quantity (from the practical engineering point of view), i.e., the

instant at which the power law starts governing the evolution of the F-function, is almost insensitive to the approach adopted (i.e., in terms of X or χ). The respective conclusions for all the tests of both protocols are almost identical.

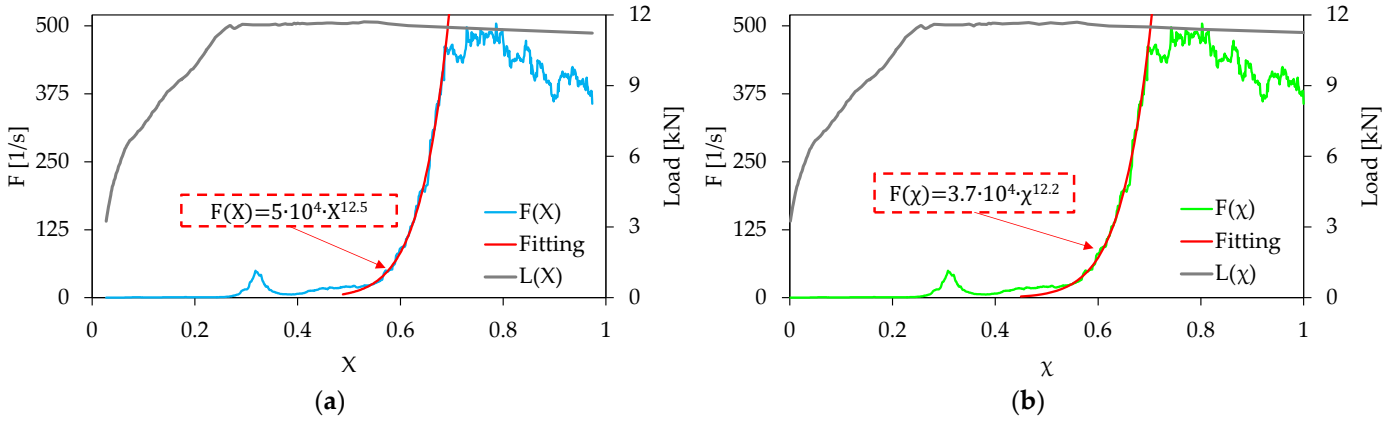


Figure 14. The evolution of the F-function, in terms of the X- (**a**) or in terms of the χ- (**b**) parameter, for the unreinforced beam, R0.

Table 2. The numerical values of the fitting parameters A and m.

Sample	$\mathbf{F(X)=A\cdot X^m}$		$\mathbf{F(\chi)=A\cdot \chi^m}$	
	A	**m**	**A**	**m**
LR1	269	8.0	247	8.0
LR2	193	6.6	177	6.5
R0	5×10^4	12.5	3.7×10^4	12.2
RM (peak 1)	7.8×10^6	7.5	6.1×10^6	7.2
(peak 2)	687	6.9	641	6.8

5.4. Concluding Remarks

The evolution of the acoustic activity, described in terms of the rate of generation of acoustic hits using the F-function was studied in the Natural Time domain, using experimental data from two protocols with cement mortar specimens. It was concluded that, at the last loading stages (namely for loads which approach the ones that are responsible for macroscopic fracture), the evolution of the F-function, analyzed in the Natural Time domain, is governed by a specific power law, independently of the geometry of the specimens and the loading protocol.

A similar behavior was observed very recently [13] in protocols with marble specimens of various geometries under a series of loading protocols. The results of the present study definitely support the conclusions drawn in ref. [13].

The critical "instant" X, at which the F-function starts exhibiting an intense increasing trend (in terms of the Natural Time), obeying the $F(X) \propto X^m$ law, properly combined with the respective values of the load levels attained, suggests clearly that the specimen is about to enter into its critical stage (that of impending macroscopic fracture), providing, thus, a potentially valuable pre-failure indicator.

It was concluded that, at the last loading stages (namely for loads which approach the ones that are responsible for macroscopic fracture), the evolution of the F-function, analyzed in the Natural Time domain, is governed by a specific power law, at least for the geometries and loading protocols of the present study. Obviously, more complicated structures should also be studied, in order to further validate the aforementioned findings, in the direction of drawing definite conclusions about the suitability of the critical "instant" X as a safe pre-failure indicator. In this direction, the evolution of additional quantities in

the Natural Time Domain is considered by the authors' team, and their study is in progress. As an indicative example one can mention the evolution of the cumulative counts, which is plotted in Figure 15, in juxtaposition to the respective evolution of the F(χ) function.

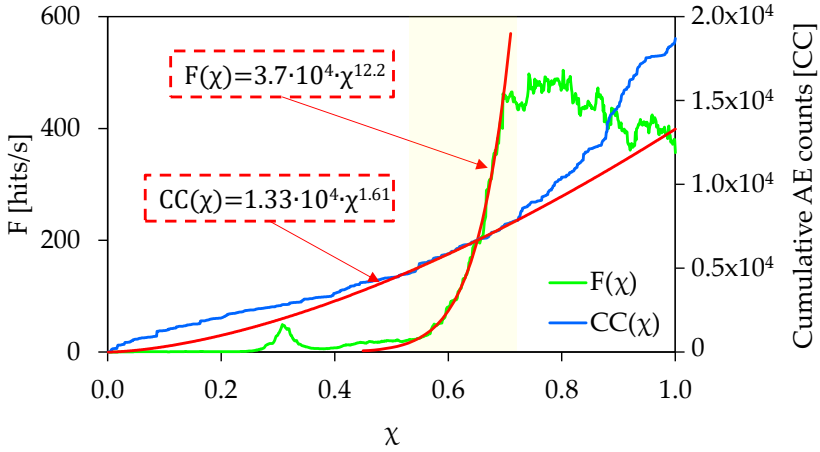


Figure 15. The evolution of the F-function, in terms of the χ parameter, in juxtaposition to the respective evolution of the cumulative counts for the unreinforced beam, R0.

It is clearly seen that a power law, similar to the one governing the evolution of the F(χ) function, governs also the evolution of the cumulative counts in the same interval of χ-values. In any case, the specific issue concerns researchers worldwide [34,35] and is still under intensive study.

Author Contributions: Conceptualization, D.T.; Methodology, D.T. and S.K.K.; Investigation, I.S., A.L. and E.D.P.; Writing–original draft, D.T. and S.K.K.; Writing–review & editing, I.S., E.D.P. and S.K.K.; Visualization, A.L. and E.D.P.; Supervision, D.T. and S.K.K. All authors have read and agreed to the published version of the manuscript.

Funding: This research received no external funding.

Institutional Review Board Statement: Not applicable.

Informed Consent Statement: Not applicable.

Data Availability Statement: All raw data used in this study are available upon request.

Conflicts of Interest: The authors declare no conflict of interest.

References

1. Grosse, C.U.; Ohtsu, M. *Acoustic Emission Testing*; Springer: Berlin/Heidelberg, Germany, 2008.
2. Grosse, C.U. Introduction. In *Acoustic Emission Testing*; Grosse, C.U., Ohtsu, M., Aggelis, D.G., Shiotani, T., Eds.; Springer Tracts in Civil Engineering; Springer: Cham, Switzerland, 2022.
3. Sagar, R.V.; Prasad, B.K.R. A review of recent developments in parametric based acoustic emission techniques applied to concrete structures. *Nondestruct. Test. Eval.* **2012**, *27*, 47–68. [CrossRef]
4. Aggelis, D.G.; Soulioti, D.V.; Sapouridis, N.; Barkoula, N.M.; Paipetis, A.S.; Matikas, T.E. Acoustic emission characterization of the fracture process in fibre reinforced concrete. *Constr. Build. Mater.* **2011**, *25*, 4126–4131. [CrossRef]
5. Vidya Sagar, R.; Prasad, R.V.; Raghu Prasad, B.K.; Rao, M.V.M.S. Microcracking and fracture process in cement mortar and concrete: A comparative study using acoustic emission technique. *Exp. Mech.* **2013**, *53*, 1161–1175. [CrossRef]
6. Kourkoulis, S.K.; Pasiou, E.D.; Dakanali, I.; Stavrakas, I.; Triantis, D. Notched marble plates under tension: Detecting pre-failure indicators and predicting entrance to the "critical stage. *Fatigue Fract. Eng. Mater. Struct.* **2018**, *41*, 776–786. [CrossRef]
7. Triantis, D.; Kourkoulis, S.K. An alternative approach for representing the data provided by the acoustic emission technique. *Rock Mech. Rock Eng.* **2018**, *51*, 2433–2438. [CrossRef]
8. Triantis, D.; Pasiou, E.D.; Stavrakas, I.; Kourkoulis, S.K. Hidden affinities between electric and acoustic activities in brittle materials at near-fracture load levels. *Rock Mech. Rock Eng.* **2022**, *55*, 1325–1342. [CrossRef]
9. Zhang, J.-Z.; Zhou, X.-P.; Zhou, L.-S.; Berto, F. Progressive failure of brittle rocks with non-isometric flaws: Insights from acousto-optic-mechanical (AOM) data. *Fatigue Fract. Eng. Mater. Struct.* **2019**, *42*, 1787–1802. [CrossRef]

10. Wang, X.; Wang, E.; Liu, X. Damage characterization of concrete under multi-step loading by integrated ultrasonic and acoustic emission techniques. *Constr. Build. Mater.* **2019**, *221*, 678–690. [CrossRef]
11. Ge, Z.; Sun, Q. Acoustic emission characteristics of gabbro after microwave heating. *Int. J. Rock. Mech. Min.* **2021**, *138*, 104616. [CrossRef]
12. Huang, J.; Liao, Z.; Hu, Q.; Song, Z.; Wang, X. Fracture mechanism of tight sandstone under high and complex 3-D stress compression: Insights from acoustic emission. *J. Petrol. Sci. Eng.* **2022**, *208*, 109635. [CrossRef]
13. Loukidis, A.; Triantis, D.; Stavrakas, I.; Pasiou, E.D.; Kourkoulis, S.K. Detecting criticality by exploring the acoustic activity in terms of the "Natural-Time" concept. *Appl. Sci.* **2022**, *12*, 231. [CrossRef]
14. Varotsos, P.A.; Sarlis, N.V.; Skordas, E.S. Spatio-temporal complexity aspects on the interrelation between seismic electric signals and seismicity. *Proc. Athens Acad.* **2001**, *76*, 294–321.
15. Varotsos, P.A.; Sarlis, N.V.; Skordas, E.S. Long-range correlations in the electric signals that precede rupture. *Phys. Rev. E* **2002**, *66*, 011902. [CrossRef]
16. Varotsos, P.A.; Sarlis, N.V.; Skordas, E.S. Attempt to distinguish electric signals of a dichotomous nature. *Phys. Rev. E* **2003**, *68*, 031106. [CrossRef]
17. Varotsos, P.A.; Sarlis, N.V.; Skordas, E.S. Natural time analysis: The new view of time. In *Precursory Seismic Electric Signals, Earthquakes and Other Complex Time-Series*; Springer: Berlin/Heidelberg, Germany, 2011.
18. Vallianatos, F.; Michas, G.; Benson, P.; Sammonds, P. Natural time analysis of critical phenomena: The case of acoustic emissions in triaxially deformed Etna basalt. *Phys. A* **2013**, *392*, 5172–5178. [CrossRef]
19. Hloupis, G.; Stavrakas, I.; Vallianatos, F.; Triantis, D. A preliminary study for prefailure indicators in acoustic emissions using wavelets and natural time analysis. *Proc. Inst. Mech. Eng. Part L J. Mater. Des. Appl.* **2016**, *230*, 780–788. [CrossRef]
20. Kourkoulis, S.K.; Pasiou, E.D.; Loukidis, A.; Stavrakas, I.; Triantis, D. Comparative assessment of criticality indices extracted from acoustic and electrical signals detected in marble specimens. *Infrastructures* **2022**, *7*, 15. [CrossRef]
21. Loukidis, A.; Perez-Oregon, J.; Pasiou, E.D.; Kourkoulis, S.K.; Sarlis, N.V.; Triantis, D. Natural time analysis of acoustic emissions before fracture: Results compatible with the Bak-Tang-Wiesenfeld model. *Europhys. Lett.* **2022**, *139*, 12004. [CrossRef]
22. Niccolini, G.; Potirakis, S.M.; Lacidogna, G.; Borla, O. Criticality hidden in acoustic emissions and in changing electrical resistance during fracture of rocks and cement-based materials. *Materials* **2020**, *13*, 5608. [CrossRef]
23. Loukidis, A.; Pasiou, E.D.; Sarlis, N.V.; Triantis, D. Fracture analysis of typical construction materials in natural time. *Phys. A Stat. Mech. Appl.* **2020**, *547*, 123831. [CrossRef]
24. Loukidis, A.; Pasiou, E.D.; Sarlis, N.V.; Triantis, D. Similarity of fluctuations of acoustic emissions in natural time. *Procedia Struct. Integr.* **2020**, *25*, 195–200. [CrossRef]
25. Loukidis, A.; Perez-Oregon, J.; Pasiou, E.D.; Sarlis, N.V.; Triantis, D. Similarity of fluctuations in critical systems: Acoustic emissions observed before fracture. *Phys. A Stat. Mech. Appl.* **2021**, *566*, 125622. [CrossRef]
26. Friedrich, L.F.; Cezar, É.S.; Colpo, A.B.; Tanzi, B.N.R.; Sobczyk, M.; Lacidogna, G.; Niccolini, G.; Kosteski, L.E.; Iturrioz, I. Long-range correlations and natural time series analyses from acoustic emission signals. *Appl. Sci.* **2022**, *12*, 1980. [CrossRef]
27. Gadhiya, S.; Patel, T.N.; Shah, D. Bendable concrete: A review. *Int. J. Struct. Civ. Eng. Res.* **2015**, *4*, 141–147.
28. Sivakumar, A.; Santhanam, M. Mechanical properties of high strength concrete reinforced with metallic and non-metallic fibres. *Cement Concrete Comp.* **2007**, *29*, 603–608. [CrossRef]
29. Ahmad, S.; Umar, A. Fibre-reinforced self-compacting concrete: A review. In *IOP Conference Series: Materials Science and Engineering*; IOP Publishing: Bristol, UK, 2018; Volume 377.
30. RamyaSree, P.; Chandra, A.; Bhasker, M.; Swami, B.L.P. Study of compressive and flexural strength of fibrous triple blended high strength concrete with fly ash and condensed silica fume. *Int. J. Res. Eng. Technol.* **2015**, *4*, 149–155.
31. Qureshi, A.U. *Advances in Civil Engineering Materials*; Concepts Books Publication: Sagar, India, 2022.
32. Sathish Kumar, V.; Ganesan, N.; Indira, P.V.; Murali, G.; Vatin, N.I. flexural behaviour of hybrid fibre-reinforced ternary blend geopolymer concrete beams. *Sustainability* **2022**, *14*, 5954. [CrossRef]
33. Loukidis, A.; Stavrakas, I.; Triantis, D. Electrical methods for sensing damage in cement mortar beams combined with acoustic emissions. *Materials* **2022**, *15*, 4682. [CrossRef]
34. Chai, M.; Hou, X.; Zhang, Z.; Duan, Q. Identification and prediction of fatigue crack growth under different stress ratios using acoustic emission data. *Int. J. Fatigue* **2022**, *160*, 106860. [CrossRef]
35. Ozevin, D.; Kessler, S. The dependence of acoustic emission behavior on prior fatigue loading history. *Front. Built Environ.* **2022**, *8*, 981327. [CrossRef]

Disclaimer/Publisher's Note: The statements, opinions and data contained in all publications are solely those of the individual author(s) and contributor(s) and not of MDPI and/or the editor(s). MDPI and/or the editor(s) disclaim responsibility for any injury to people or property resulting from any ideas, methods, instructions or products referred to in the content.